Biocompatibility of sol-gel hydroxyapatite-titania composite and bilayer coatings

D. Sidane [a,*,1], H. Rammal [b,1], A. Beljebbar [c], S.C. Gangloff [b], D. Chicot [d], F. Velard [b], H. Khireddine [a], A. Montagne [e], H. Kerdjoudj [b]

[a] Laboratoire de Génie de l'Environnement (LGE), Faculté de Technologie, Université de Bejaia, 06000, Bejaia, Alegria
[b] Equipe d'Accueil 4691 Biomatériaux et Inflammation en Site Osseux, SFR-CAP Santé (FED 4231), Université de Reims Champagne Ardenne, 1 Avenue du Maréchal Juin, 51100 Reims, France
[c] UMR CNRS 7369, Equipe MéDIAN Biophotonique et Technologies pour la Santé, UFR de Pharmacie, SFR-CAP Santé (FED 4231), Université de Reims Champagne Ardenne, 51 rue Cognacq-Jay, 51096 Reims, France
[d] FRE 3723 - LML - Laboratoire de Mécanique de Lille, Univ. Lille, 59000 Lille, France
[e] MSMP, Arts et Métiers Paris Tech, 8, Boulevard Louis XIV, 59046 Lille Cedex, France

ARTICLE INFO

Article history:
Received 18 September 2016
Received in revised form 9 November 2016
Accepted 26 November 2016
Available online 5 December 2016

Keywords:
Stainless steel 316L
Surface coating
Hydroxyapatite
Titania
Stem cells
Biocompatibility

ABSTRACT

Titania-Hydroxyapatite (TiO_2/HAP) reinforced coatings are proposed to enhance the bioactivity and corrosion resistance of 316L stainless steel (316L SS). Herein, spin- and dip-coating sol-gel processes were investigated to construct two kinds of coatings: TiO_2/HAP composite and TiO_2/HAP bilayer. Physicochemical characterization highlighted the bioactivity response of the TiO_2/HAP composite once incubated in physiological conditions for 7 days whereas the TiO_2/HAP bilayer showed instability and dissolution. Biological analysis revealed a failure in human stem cells adhesion on TiO_2/HAP bilayer whereas on TiO_2/HAP composite the presence of polygonal shaped cells, possessing good behaviour attested a good biocompatibility of the composite coating. Finally, TiO_2/HAP composite with hardness up to 0.6 GPa and elastic modulus up to 18 GPa, showed an increased corrosion resistance of 316L SS. In conclusion, the user-friendly sol-gel processes led to bioactive TiO_2/HAP composite buildup suitable for biomedical applications.

1. Introduction

In recent years, the progress in surgical techniques has led to a marked growth in the use of biomaterials for advanced medical devices and implants. Metallic materials such as 316L stainless steel (316L SS), Cobalt–Chrome alloys, titanium (Ti) and alloys (Ti–6Al–4V) are widely used biomaterials for hard tissue replacement due to their superior tensile, strength, fracture toughness, corrosion resistance and biocompatibility within the human environment [1]. 316L SS is commonly used in orthopedic medical field due to its favourable combination of mechanical properties, biocompatibility, cost effectiveness and of corrosion resistance [2,3]. This latter is due to the presence of a passive thin oxide film on its surface, which however, may still allow a significant release of toxic ions such as nickel, causing pain and hampering thereby implants biocompatibility and integration [4,5].

To improve 316L SS implants corrosion resistance and long-term biocompatibility, various surface functionalization techniques have been proposed [6]. Owing to its remarkable features, biomimetic hydroxyapatite (HAP), calcium phosphate mineral with chemical composition close to bone, was deposited onto metal implants using plasma-spraying [7], pulsed laser deposition [8] and electrophoretic deposition [9]... among these techniques, only plasma-spraying has achieved commercial success for clinical applications. Despite excellent biocompatibility and bone integration, some drawbacks including instability and high thickness, heterogeneous composition, highly crystalline and poor bioactive interface have been noticed regarding the long-term performance of the resulting HAP coatings [2,10].

Sol-gel synthesis of HAP for implant coatings, using dip- [11,12] and spin-coating [13] processes has recently attracted much attention [14,15]. Based on mixing calcium and phosphorus precursors, these processes do not require sophisticated equipment and are potentially less expensive compared to above cited conventional techniques. This versatile approach offers several advantages, e.g. low processing temperatures, better control of the chemical composition and microstructure, possibility of preparing homogeneous surfaces, adaptability to coat complex implant shapes and a good bioactivity due to the presence of many hydroxyl groups promoting calcium and phosphate precipitation and improving the interactions with cells such as osteoblasts [16,17]. Unfortunately, a poor adhesion of biomimetic HAP to the 316L SS is

* Corresponding author at: Université Abderrahmane Mira, Route Targa Ouzemour, 06000 Bejaia, Algeria.
E-mail address: dj.sidane@yahoo.fr (D. Sidane).
[1] Both authors contributed equally to this work.

still a common disadvantage. To achieve this issue, reinforcement with inner titania (TiO_2) layer has been proposed to improve the corrosion resistance, mechanical strength and chemical stability of HAP-coated 316L SS. As a result, the combination of biomimetic HAP and TiO_2 reinforcement acts as an effective barrier for 316L SS implant corrosion in physiological fluid [11,18].

Accordingly, the aim of this work is to combine dip- and spin-coating processes in order to generate two types of 316L SS coating: (i) TiO_2/HAP bilayer, formed by separate deposition of respectively inner TiO_2 and outer HAP and (*ii*) TiO_2/HAP composite, formed by a mixture of TiO_2/HAP. Physicochemical, corrosion resistance and mechanical features of the resulting coatings under physiological conditions were investigated. In addition, stem cell response to both coatings was also studied.

2. Experimental

2.1. Hydroxyapatite-titania coatings preparation

Phosphorus pentoxide (P_2O_5, Prolabo 100%) and calcium nitrate tetrahydrate ($Ca(NO_3)_2.4H_2O$, Fluka 98%) were dissolved in absolute ethanol to form two solutions with concentrations of 0.5 M and 1.67 M, respectively. These solutions were mixed to obtain hydroxyapatite (HAP) sol with a Ca/P molar ratio of 1.67 [19]. The mixture was continuously stirred at room temperature for 24 h. Titanium isopropoxide (TIP, Fluka 100%) was used as titania (TiO_2) precursor in the sol–gel process. The reactivity toward water was modified by acetic acid (HOAc) (molar ratio of TIP/HOAc = 1/10), also used as catalyst. Thereafter, 2-methoxy ethanol was added to adjust the degree of viscosity of the solution. This solution with TIP molar concentration of approximately 0.47 M was vigorously stirred at room temperature [20].

316L stainless steel (316L SS) (20 × 10 × 2 mm) used as receiving surface, were degreased with acetone, washed with running double distilled water and dried at 150 °C for 10 min. 316L SS were mechanically polished using different silicon carbide grit papers from 120 to 1200 grades and diamond paste of 2 and 0.7 μm in the final step, then degreased again, washed and dried.

Related to the preparation of TiO_2/HAP composite coating, TiO_2 and HAP solutions were mixed with a volume of 20 and 80 (vol.%), respectively and continuously stirred for 14 h. After TiO_2/HAP composite layer was obtained by spin-coating at a speed of 2000 rpm for 10 s, spin-coated 316L SS were then transferred into an air oven, held at 150 °C for 15 min, and annealed at 500 °C for 60 min in air. Subsequently, the coated–316L SS was dipped in the suspension with a dipping rate of 80 mm/min, dried and annealed as previously described. For the preparation of the TiO_2/HAP bilayer coating, TiO_2 and HAP sols were closely capped and aged for 24 h at room temperature and 100 °C, respectively. TiO_2 inner layer was obtained by spin-coating at a speed of 2000 rpm for 10 s, the coated 316L SS was then dried and annealed at 450 °C for 60 min. HAP outer layer was deposited onto the surface of the TiO_2 inner layer with dipping rate of 80 mm/min then dried and annealed at 500 °C for 60 min in air.

2.2. Physicochemical, electrochemical and mechanical characterization

TiO_2/HAP bilayer and composite coatings were soaked in alpha-Minimal Eagle Medium (α-MEM, Lonza) at 37 °C for 7 days and investigated by:

2.2.1. Profilometry analysis using a "DEKTAK 150 SURFACE PROFILERT"

The surface of the coating is scanned at an interval of 1000–8000 μm. Three different areas were scanned and measured to determine a mean value for the thickness and roughness.

2.2.2. Near infrared confocal Raman spectrometer (Labram ARAMIS, Horiba Jobin Yvon S.A.S., France) coupled to a microscope (100 × optimized objective Olympus, BX41, France) using excitation source at 785 nm

All spectra were acquired using a 20 s integration time in the 100–1800 cm^{-1} spectral region with a spectral resolution of 4 cm^{-1}. Data acquisition was carried out by means of the LabSpec 5 software (Horiba Jobin Yvon S.A.S. France). Data pretreatment consisted of cosmic ray removal, wavenumber calibration, instrument response correction, and CaF_2 interference subtraction. All spectra were baseline corrected using a fourth order polynomial and smoothed with 7 points Savitzky-Golay algorithm in order to minimise the influence of noises. The resulting spectra were then normalized using a standard normal variate (SNV) procedure [21].

2.2.3. Scanning electron microscopy-energy dispersive X-ray spectroscopy (SEM-EDX, JEOL JSM 6010LA)

The X-ray spectra were acquired at primary beam energy of 10 keV with an acquisition time of 30 s.

2.2.4. X-ray diffractometer (panalytical type MPD/system vertical θ/θ)

The X-ray pattern data was collected from 2θ = 20° to 80° using incremental step size of 0.02° with 59 s of acquisition time per step.

2.2.5. Potentiodynamic cyclic voltammetry tests using a Voltalab equipment (serial: 913V708/INT), interfaced with a computer and loaded with VoltaMaster 4 software

A platinum electrode was used as the auxiliary electrode and the saturated calomel electrode (SCE) was used as the reference electrode. Corrosion potential (E_{Corr}), and corrosion current density (I_{Corr}) were determined using the Tafel diagram with sweeping potential from −1000 to +1000 mV at the rate of 1 mVs^{-1}, all tests were carried out on several samples and, at least, three similar results were required to ensure reproducibility.

2.2.6. Nano Indenter XP™ (MTS Nano Instruments) with a Berkovich diamond indenter

316L SS coated samples were fixed on a metallic support using the heat softening glue crystalbond 509. 25 indentation tests were conducted randomly on the surface of the material with the same indentation testing conditions. The maximum indentation depth reached by the indenter was fixed at 2000 nm and the strain rate was equal to 0.05 s^{-1}. The instrument was operated in the continuous stiffness measurement (CSM) mode allowing the computation of the elastic modulus and the hardness continuously during the indentation loading. The harmonic displacement was 2 nm and the frequency was 45 Hz. The elastic modulus of the coating, E_C, is deduced from the reduced modulus, E_{RC}, given by the instrument, which takes into account the elastic properties, E_i and ν_i, related to the indenter material and the Poisson's ratio of the coating, ν_c:

$$E_C = \left(1-\nu_c^2\right)\left[\frac{1}{E_{RC}} + \frac{\left(1-\nu_i^2\right)}{E_i}\right]^{-1} \quad (1)$$

For a diamond indenter, the elastic modulus, E_i, and the Poisson's coefficient, ν_i, are equal to 1140 GPa and 0.07, respectively [22]. ν_c is taken equal to the mean value of 0.3 because the analysis deals with a multilayered coating.

For thin films, the substrate can interfere with the mechanical property measurement. Consequently, a model must be applied for separating the influence of the substrate on the measurement. Perriot and Barthel [23] proposed the empirical model in Eq. (2) which represents the measured reduced modulus, E_{RC}, as a function of E_{RF} (obtained for the lowest loads and representing the reduced modulus of the film) and E_{RS} (obtained for the highest loads and representing the reduced

modulus of the substrate):

$$E_{RC}\left(\frac{a}{t}\right) = E_{RF} + \frac{(E_{RS} - E_{RF})}{1 + \left(\frac{tx_0}{a}\right)^n} \quad (2)$$

where x_0 and n are adjustable constants. The parameter x_0 is the value of the a/t ratio for which $E_{RC} = (E_{RS} + E_{RF}) / 2$. At the same time it corresponds to the change in curvature of the (E_{RC}; a/t) curve plotted in semi-log coordinates.

2.3. Biological tests

Human umbilical cords were harvested at the maternity of the University Hospital Center (CHU) of Reims, according to the guidelines approved by the ethical board of the CHU, in accordance with French Article R 1243-57 and written non-opposition consent of the mothers. All procedures were done in accordance with the authorization and registration number DC-2014-2262 given by the French National "Cellule de Bioéthique". Stem cells, enzymatically isolated from fresh human umbilical cords obtained after full-term births [24], were cultured in complete culture medium [alpha-Minimal Eagle Medium (α-MEM, Lonza) supplemented with 10% decomplemented fetal bovine serum (FBS), 1% Penicillin/Streptomycin/Amphotericin B and 1% Glutamax® (v/v, Gibco)] and used in our experimental procedure at the 4th passage (P4).

Autoclaved TiO_2/HAP bilayer, TiO_2/HAP composite and 316L SS were placed in 12 well plates. Stem cells were seeded on the top of substrates at 10^4 cells/cm^2 and maintained in complete culture medium for 9 days.

2.3.1. WST 1 cell proliferation assay (Roche Diagnostics, France) performed after 4, 7 and 9 days of stem cell culture

Absorbance was measured at 490 nm using a FLUOstar Omega microplate reader (BMG Labtech) against a background control as blank. A wavelength of 750 nm was used as the reference wavelength.

2.3.2. Cytoskeleton staining with Alexa® Fluor-488 conjugated-Phalloidin® (Invitrogen)

After 9 days of culture, stem cells were fixed with 4% (w/v) paraformaldehyde for 15 min at room temperature, permeabilized with 0.5% (v/v) Triton X-100 for 15 min and finally stained with Alexa® Fluor-488 conjugated-Phalloidin® (Invitrogen, 1/100) for 30 min. Nuclei were counter-stained with 4,6-diamidino-2-phenylindole (DAPI, 100 ng/mL, 1:10,000 dilution) for 5 min. Stained cells were then mounted and imaged by fluorescence microscopy (Zeiss microscopy, ×20).

2.3.3. Scanning electron microscopy (JEOL JSM 6010LA)

After 9 days of culture, stem cells were fixed in 2.5% (w/v) glutaraldehyde (Sigma-Aldrich) at room temperature 37 °C for 1 h. Cells were dehydrated in graded ethanol solutions from 50 to 100% and in hexamethyldisilazane (HMDS, Sigma) for 10 min. After air-drying at room temperature, samples were sputtered with a thin gold–palladium film under a JEOL ion sputter JFC 1100, before being observed with a LaB6 electron microscope (JEOL JSM-5400 LV).

2.4. Statistical analysis

Data are presented as mean ± SEM for each condition. TiO_2/HAP composite and bilayer characterizations were accomplished in triplicate and comparisons were performed using non parametric Mann & Whitney test. Biological test were done using three independent donors. For each donor and each experimental condition, WST-1® was performed in triplicate and an unpaired T-student test was then applied (GraphPad Prism 5 software). For each test a value of $p < 0.05$ was accepted as statistically significant p (rejection level of the null-hypothesis of equal means).

3. Results and discussion

Chemical and physical properties of TiO_2/HAP bilayer and composite coatings, including thickness, roughness, homogeneity and bioactivity constitute critical parameters for biocompatibility. Due to high chemical and thermal stability of TiO_2 and HAP [25], this study is focused on TiO_2:HAP with fixed ratio 20:80. To evaluate the performance and the bioactivity of the resulting coatings, all investigations were assessed on TiO_2/HAP bilayer and composite deposited on 316L SS soaked in a culture medium for 7 days at 37 °C, as previously described [26,27]. This incubation period is shown to be enough to promote the formation of bone-*like* apatite layer on the surface of the HAP coatings containing TiO_2 [28–30].

3.1. Physical and morphological characterization

The structural characteristics of TiO_2/HAP bilayer and composite coated 316L SS in term of thickness and roughness are summarized in Table 1. Both coatings exhibited structured surfaces with 1149 ± 58 and 761 ± 37 nm of roughness for TiO_2/HAP bilayer and composite, respectively. After 7 days of incubation in culture medium, we noticed decrease (<1000 nm, $p = 0.1$, Mann & Whitney test) of TiO_2/HAP bilayer roughness whereas no significant changes of surface roughness were observed on the TiO_2/HAP composite (≈700 nm, $p = 0.2$ Mann & Whitney test). The thickness of both coatings is estimated by profilometry analysis and the obtained values were about 3 μm and 2.6 μm for bilayer and composite, respectively, with no significant variations after culture medium incubation ($p = 0.4$ and $p = 0.1$, Mann & Whitney test, for respectively composite and bilayer). When considering translational applications, the use of dip- and spin-coating processes seems to be favoured to design thin coatings < 10 μm, required for orthopedic and dental implants [31]. The scanning electron microscopy (SEM) micrographs showed an irregular and heterogeneous coating for TiO_2/HAP bilayer (Fig. 1a) whereas a uniform coating was obtained for the TiO_2/HAP composite (Fig. 1c). A closer SEM examination showed that HAP exhibits various sized clusters (Fig. 1b, yellow arrow) and granular-*like* particles (Fig. 1b, red arrow) for TiO_2/HAP bilayer, in accordance with Kim et al., data obtained on TiO_2/HAP deposited on titanium [25], whereas needle-*like* particles are displayed on TiO_2/HAP composite (Fig. 1d, blue arrows). The needle-*like* morphology is thought to provide a high surface area and to possess higher bioactivity [32]. After 7 days of incubation in culture medium, while at lower SEM magnification both TiO_2/HAP bilayer (Fig. 1e) and composite (Fig. 1g) showed smoother surfaces, the higher magnification highlighted the modifications of the surface morphology. Indeed, more distinguishable nano-granular morphology was observed on TiO_2/HAP bilayer (Fig. 1f, red dashed arrows) whereas on TiO_2/HAP composite there was a switch form needle-*like* to granular-*like* structure (Fig. 1g, red arrows). To highlight and confirm HAP particles dispersion within the 316L SS, elemental X-ray maps obtained by SEM coupled to energy dispersive X-ray spectroscopy (SEM-EDX) were performed. Coating the 316L SS with TiO_2/HAP resulted in a decrease in elements associated with the 316L SS including Fe, Cr and Ni, while intense peaks for Ca and P appeared in TiO_2/HAP bilayer and composite with a higher Ti peak in TiO_2/HAP composite (Fig. 2, black line). After 7 days of incubation in culture media, a clear change in elements peak intensity was noticed on both coatings. An increase, especially for Ca and P peaks, was noticed for TiO_2/HAP composite

Table 1
Structural parameters of TiO_2/HAP coated 316L SS.

	Medium (α-MEM)	Bilayer	Composite
pH	7.60	7.80	7.81
Roughness (nm)	Day 0	1149 ± 58	761 ± 37
	Day 7	905 ± 52	706 ± 73
Thickness (nm)	Day 0	3158 ± 83	2672 ± 89
	Day 7	2983 ± 51	2646 ± 92

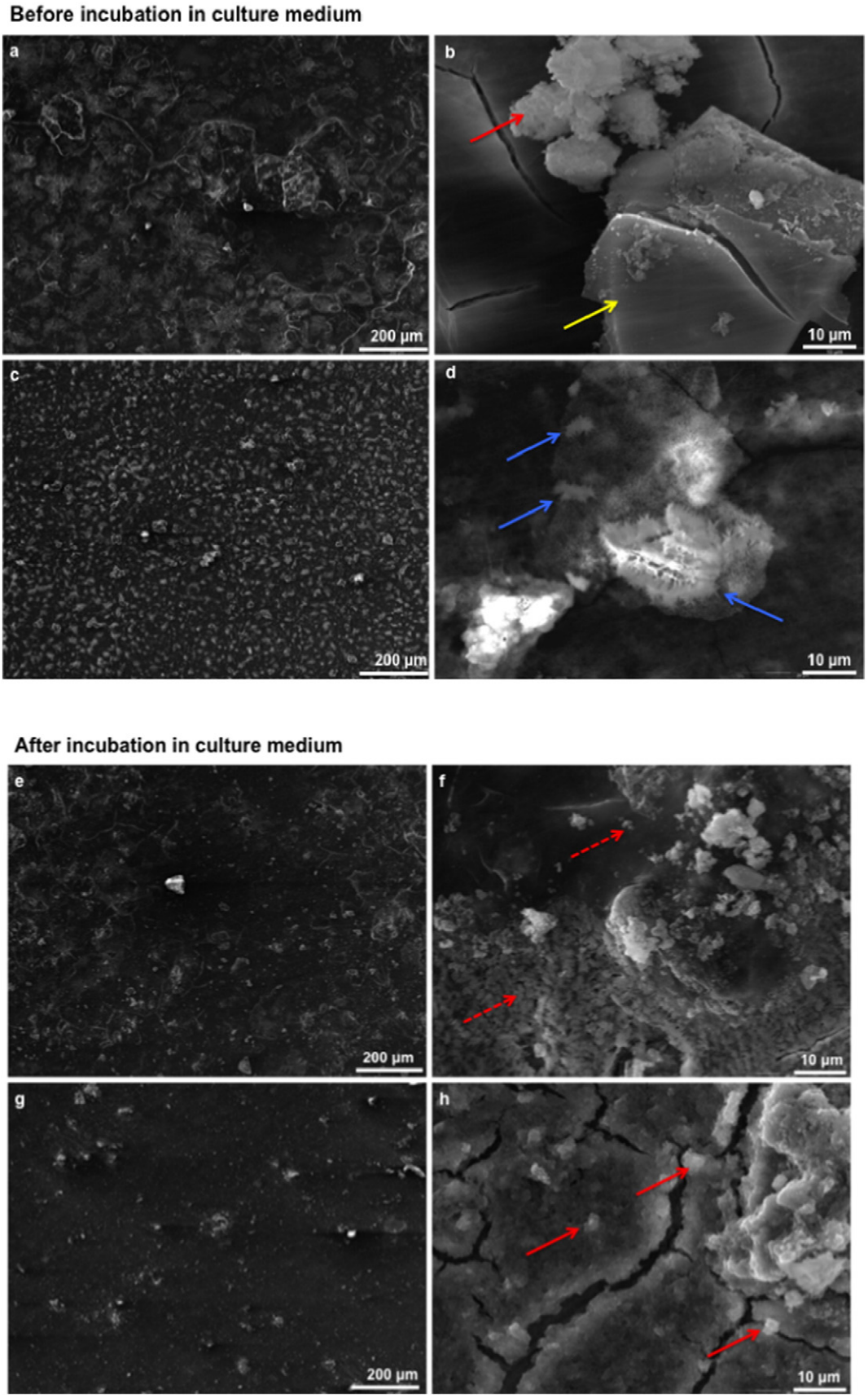

Fig. 1. Morphological characterization. Scanning electron microscopy observations of TiO_2/HAP bilayer (a, c, e and f) and composite (c, d, g and h) coated 316L SS, before (a–d) and after (e–h) 7 days of culture medium soaking (scale bar = 200 and 10 µm). Red Arrows indicate granular-*like* particles, yellow arrow indicates HAP clusters, blue arrows indicate needle-*like* particles and dashed red arrows indicate nano-granular particles.

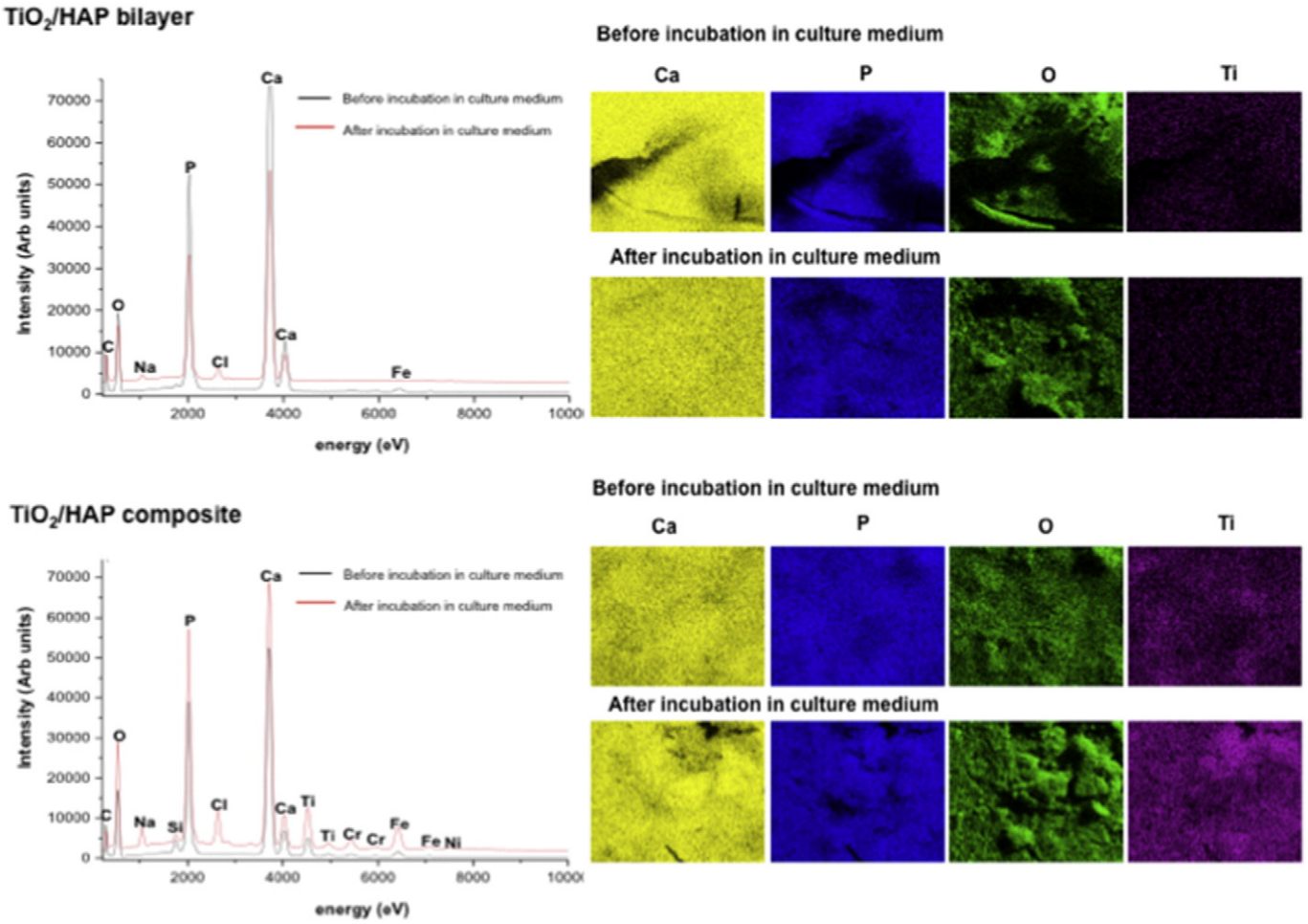

Fig. 2. Elemental X-ray map. Scanning electron microscopy - energy dispersive X-ray spectroscopy measurement of TiO_2/HAP bilayer and composite coated 316L SS, before (black line) and after (red line) 7 days of culture medium soaking.

however, a sharp decrease in both elements was observed for TiO_2/HAP bilayer (Fig. 2, red line). In spite the absence of pH variation of the culture medium (Table 1), increased Ca and P ions on TiO_2/HAP composite could be attributed to the adsorption of ions, from the culture medium, via OH^- and PO_4^{3-} ions present on the coating surface as reported previously [33]. However, decreased Ca and P on TiO_2/HAP bilayer, consisting of a crystalline inner layer of TiO_2 with a weaker crystalline layer of HAP at the outer surface, might be caused by the partially dissolution of the HAP outer layer and thus the release of both ions.

3.2. Chemical composition

Fig. 3 depicts respective patterns of the confocal Raman spectroscopy measurements and of X-ray diffractometry (XRD) of TiO_2/HAP bilayer and composite. Raman analysis of both coatings showed typical HAP vibrations $\nu_2PO_4^{3-}$ bending (O—P—O) mode at about 430–450 cm^{-1}, $\nu_1PO_4^{3-}$ symmetric stretching (P—O) mode at 960 cm^{-1}, $\nu_4PO_4^{3-}$ bending (O—P—O) mode at 585–610 cm^{-1} and $\nu_3PO_4^{3-}$ asymmetric stretching (P—O) mode at 1020–1080 cm^{-1} [34] with a single TiO_2 signature at 144 cm^{-1}, attributed to E_g modes anatase [35] (Fig. 3a and b, black line). Peak at 300 cm^{-1} is assigned to goethite of the 316L SS substrate [36]. After 7 days of incubation, differences between TiO_2/HAP bilayer and composite were clearly distinguished. While TiO_2/HAP composite did not show any variation (Fig. 3b, red line) a decrease in HAP peaks intensity and an increase in anatase peak at 144 cm^{-1} with an appearance of anatase peaks at 399, 519 and 639 cm^{-1} [35] was noticed for TiO_2/HAP bilayer (Fig. 3a, red line). The phases of TiO_2/HAP bilayer and composite were then characterized by X-ray diffractometry (XRD). According to International Center for Diffraction Data (ICDD) patterns, XRD patterns showed that besides the reflections from 316L SS (peaks at $2\theta = 44.05°$, 51.14° and 75.09°, PDF no. 00-006-0694), TiO_2/HAP bilayer and composite illustrated typical HAP diffraction peaks at $2\theta = 25.9°$, 31–32.9° and 34° (PDF no. 09-0432) and a weak peak at $2\theta = 25.35°$ corresponding to the crystallization of TiO_2 into anatase crystals (PDF no. 00-004-0477) (Fig. 3c and d, black line). Compared to the TiO_2/HAP composite, TiO_2/HAP bilayer showed sharp and narrow HAP peaks. We previously showed that the microstructural characteristics of the HAP depend on the surface features of the underlying substrate [11]. Therefore, we noticed an improvement of HAP crystallization when TiO_2 inner layer was deposited. Mixing HAP and TiO_2 in the composite is thought to delay the crystallization of HAP and thus forming weaker peaks [30]. Comparing the pattern of each coating, there were no significant differences in their behaviour after medium soaking (Fig. 3c and d, red line) despite a good development of some diffraction peaks corresponding to the TiO_2/HAP composite (Fig. 3d red line). We can also note that the main peak of TiO_2 ($2\theta = 25.35°$) is merged with the HAP peak because of their close diffraction angles and is barely visible in the TiO_2/HAP composite due to a low percentage of TiO_2 within the coating. Immersion of calcium phosphate ceramics into biological fluids involves a dissolution process immediately followed by the precipitation of a bone-*like* apatite phase, a signature of the bioactivity of the prosthetic material [17]. The bioactivity of

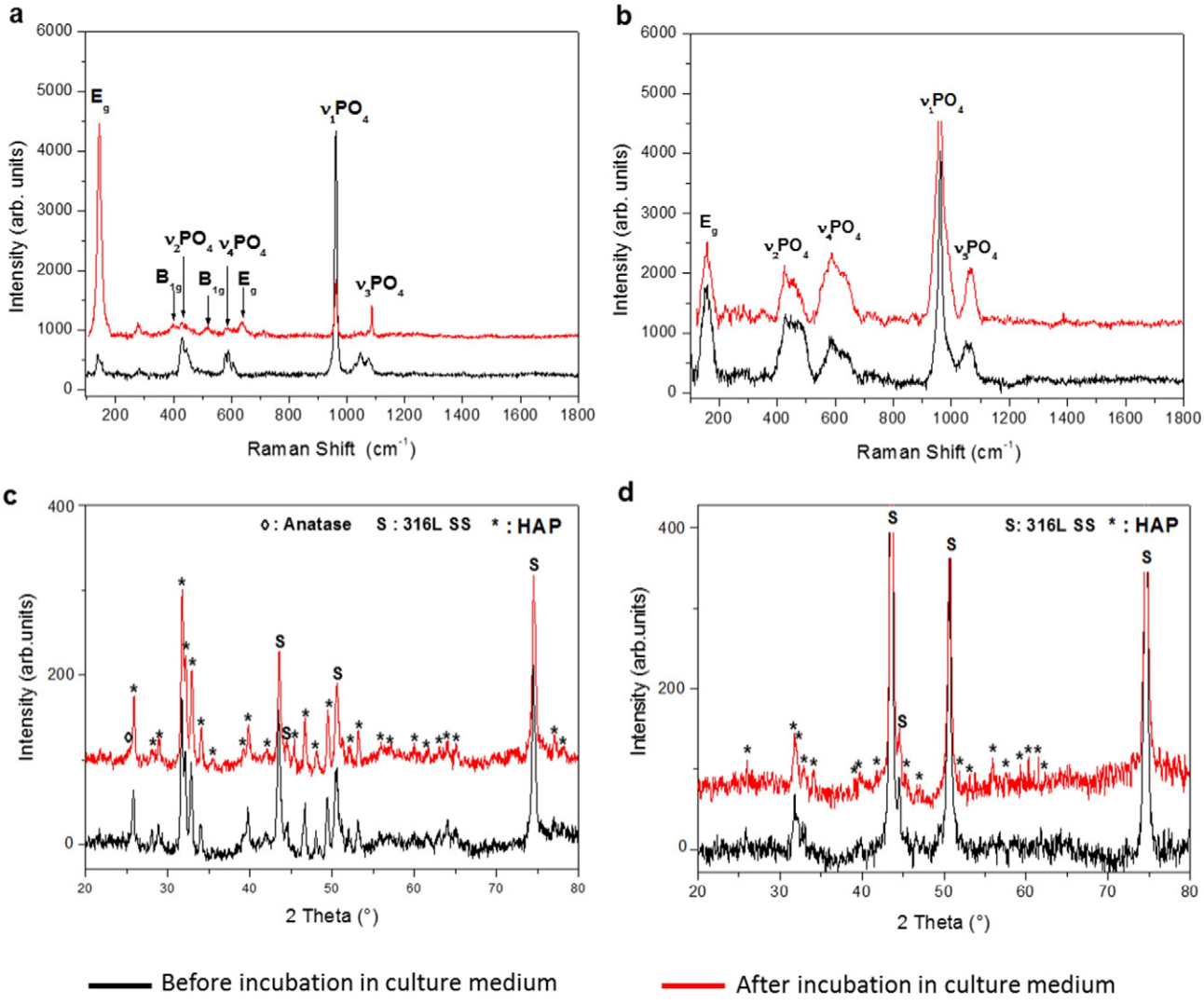

Fig. 3. Chemical composition. Raman spectrum of (a and b) and pattern of X-ray diffraction (XRD) (c and d) of TiO_2/HAP bilayer (a, c) and composite (b, d) coated 316L SS, before (black line) and after (red line) 7 days of culture medium soaking. (*) HAP, (S) 316L SS and (◊) Anatase.

TiO_2/HAP bilayer and composite was thus illustrated across structural, morphological and chemical changes observed after incubation in culture media.

3.3. Biological tests

Results of in vitro biological tests involving stem cell behaviour on both TiO_2/HAP bilayer and composite and on control (inert and biocompatible 316L SS) are summarized in Fig. 4. Cytotoxicity of both coatings was studied using the WST-1® assay and absorption values of reduced WST-1® reagent after 4, 7 and 9 days of stem cell culture are represented in the Fig. 4a. On TiO_2/HAP composite, as on control, stem cells were metabolically active with an increase of absorbance values and a plateau appearing from day 7 until day 9 for TiO_2/HAP composite whereas on 316L SS control ($p = 0.0085$ for composite versus 316L SS for 9 days, unpaired T-student test), absorbance values increased linearly from day 4 to 9. In contrast, WST-1® reagent was not reduced by stem cells cultivated on TiO_2/HAP bilayer ($p < 0.0001$ for bilayer versus composite and 316L SS for 4, 7 and 9 days, unpaired T-student test) despite the absence of toxic released substances from TiO_2/HAP bilayer (data not shown). WST-1® assay measures metabolic activity of intact viable cells and any increase of absorbance could be a result of cell proliferation over the time. Thus, these results suggest that TiO_2/HAP bilayer coating prevents stem cell attachment, whereas TiO_2/HAP composite promotes stem cell proliferation until day 7 of culture. Considering the above described results, the higher roughness of TiO_2/HAP bilayer could decrease the contact area between the cell membrane and the surface inducing a greater cellular stress on TiO_2/HAP bilayer [37,38]. Fig. 4b and c display stem cell morphologies after 9 days of culture on TiO_2/HAP coatings investigated by SEM and cytoskeleton visualization, respectively. Stem cells on TiO_2/HAP composite and 316L SS covered the entire surface whereas on TiO_2/HAP bilayer only few rounded cells were seen. On 316L SS control, cells displayed fibroblastic morphology with parallel oriented cytoskeleton, preserving then their stem cell morphology. In contrast, stem cells on TiO_2/HAP composite seemed to lose their fibroblastic morphology and had a tendency to organize themselves in a multi-layered structure. Surface topography can be sensed by cells and even the finest changes can have a large effect on stem cell behaviour including proliferation, adherence and differentiation [39,40]. In contrast with previous published works [41,42] where an improvement of the biocompatibility of HAP coating with an inner TiO_2 layer is noticed, our results showed that stem cells adhesion is impaired on TiO_2/HAP bilayer. TiO_2/HAP composite coating showed a slight promising result on stem cell behaviour when compared to

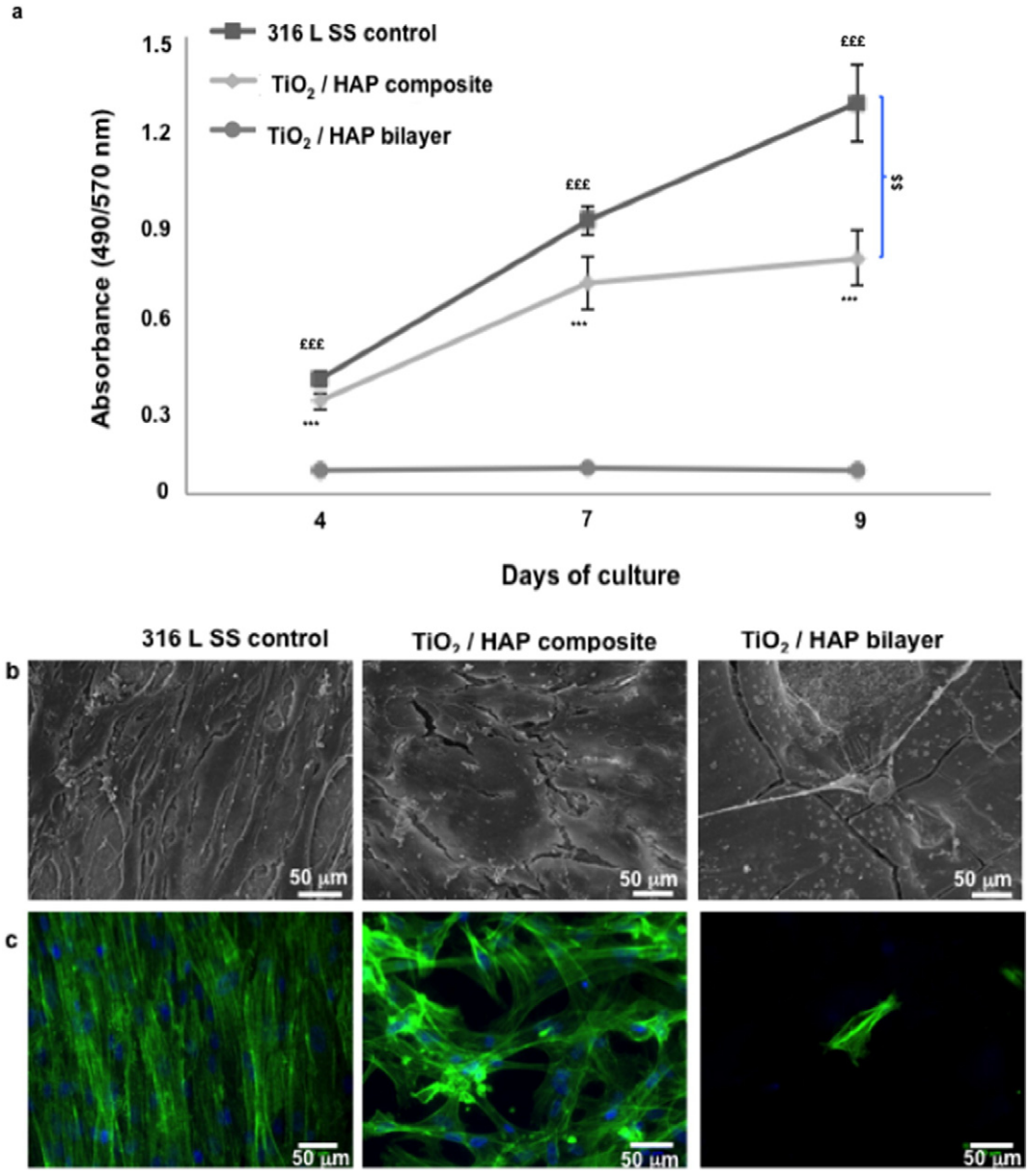

Fig. 4. Biological tests. (a) WST-1® assay after 4, 7 and 9 days of culture of stem cell on 316L SS (positive control), TiO_2/HAP composite and bilayer. The extent of metabolic cell activity was quantified by measuring the absorbance of the reduced WST-1® reagent at 490/750 nm. Values represent the mean ± S.E.M. of three independent donors performed in triplicates. (£££) $p < 0.0001$ for bilayer versus composite, (***) $p < 0.0001$ for bilayer versus 316 L SS for 4, 7 and 9 days and ($$) $p = 0.008$ for composite versus 316 L SS for 9 days, unpaired T-student test. Representative SEM (b) and cytoskeleton fluorescent (c) images of stem cells after 9 days of culture (scale bars = 50 µm).

uncoated 316L SS. Indeed, TiO_2/HAP composite delayed the proliferative state of stem cells whereas on 316L SS cells continued to proliferate after 7 days of culture and in contrast to elongated and aligned cells on 316L SS, multi-layered stem cells were observed on TiO_2/HAP composite. Taking together, our results suggest a possible stem cell proliferation/differentiation switch into bone lineage. Indeed, enhanced osteogenic differentiation in response to HAP (rough) coated surfaces was correlated to reduced cell proliferation and cell morphological changes, when compared with smooth and uncoated surfaces [43]. Further studies are required to identify whether stem cells are committed into bone forming cells.

3.4. Corrosion resistance and mechanical features investigations

316L SS steel implants are prone to localized attacks in long-term applications due to aggressive biological effects and this can be a source of some cytotoxic corrosion products affecting cell metabolism, proliferation and differentiation [44,45]. Based on the biological results, this part of the study will be focused on the TiO_2/HAP composite. Potentiodynamic cyclic voltammetry curves of TiO_2/HAP composite and uncoated 316L SS are shown in Fig. 5a. It is generally recognized that corrosion current density (I_{Corr}) represents the corrosion rate of the metallic material and the corrosion resistance of the substrate increases when the corrosion current density decreases [46]. In addition, the more positive is the value of the corrosion potential (E_{Corr}), the better is the corrosion resistance. The potentiodynamic curve of TiO_2/HAP composite is shifted toward the positive potential side, compared to uncoated 316L SS with respectively corrosion parameters ($E_{Corr} = -0.52$ V and $I_{Corr} = 0.78$ µA cm^{-2}) and ($E_{Corr} = -0.81$ V and $I_{Corr} = 1$ µA cm^{-2}); meaning that TiO_2/HAP composite seems to be more resistant to the corrosion than 316L SS. This result is thought to be related to

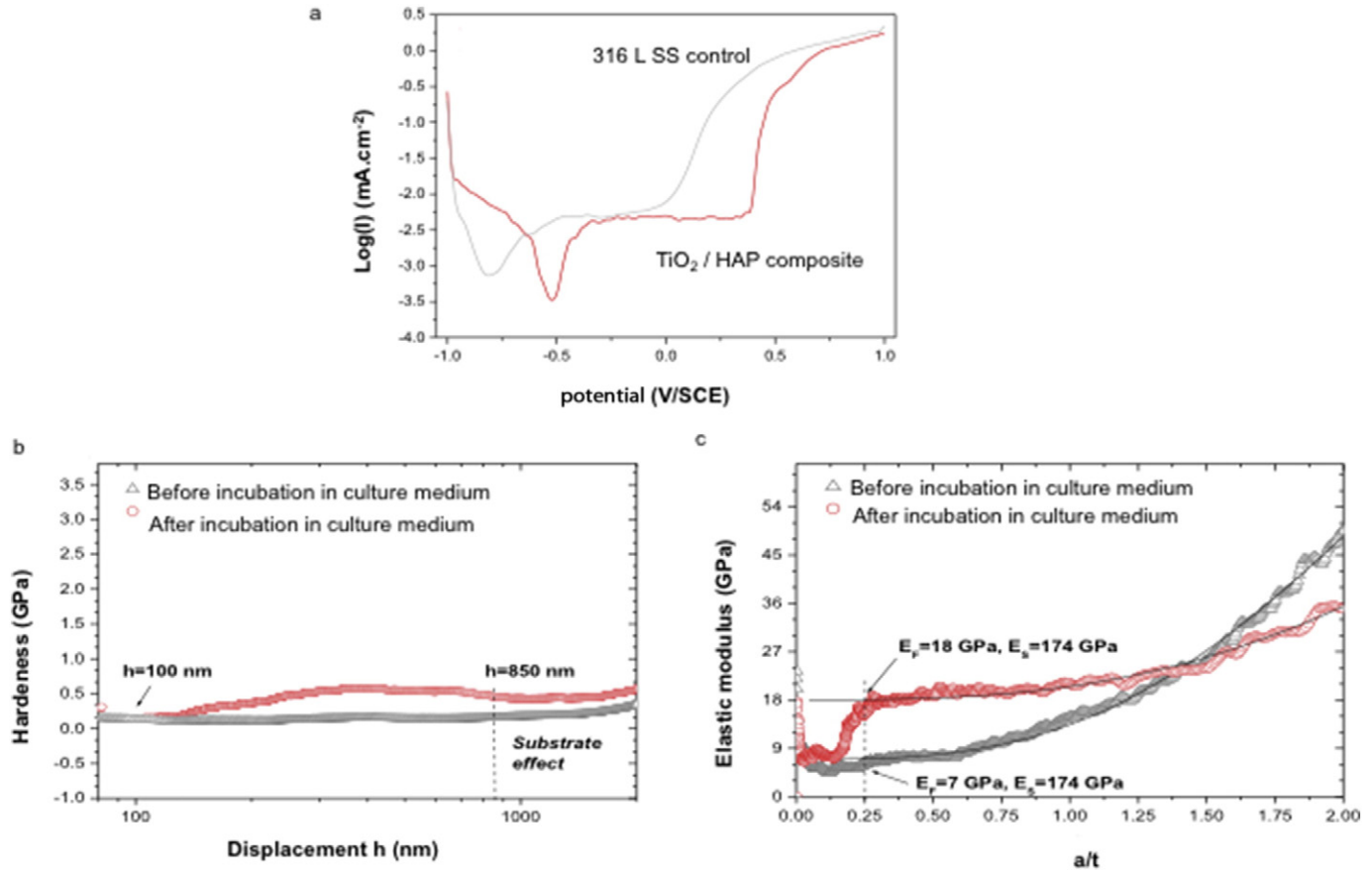

Fig. 5. Corrosion and mechanical features. (a) Potentiodynamique curves of TiO_2/HAP composite (red line) and 316L SS (black line) after 7 days of culture medium soaking. (b–c) Indentation data versus the indenter displacement applied on the TiO_2/HAP composite coating for the determination of the (b) hardness and (c) elastic modulus before (black line) and after (red line) 7 days of culture medium soaking.

the dense and compact TiO_2/HAP composite obtained upon medium soaking as previously described in Fig. 1g; acting as blocking layers against ion diffusion [18].

Besides the corrosion test, evaluating surface mechanical properties such as hardness and elastic modulus, were also performed and determined directly from indentation load and displacement measurements [47,48] and the results of surface incubation, are represented in Fig. 5b. While the hardness of the TiO_2/HAP composite revealed weak and stable values of about 0.15 GPa, its soaking in the medium for 7 days increased the hardness from 0.15 GPa at 100 nm to 0.6 GPa after 850 nm of indenter penetration. Beyond this later depth, which represents 30% of the coating thickness, the hardness measurement is more influenced by the underneath 316L SS. Despite the fact that there is no universal penetration depth beyond which the substrate effects come in, Xu and Rowcliffe [49] stated that beyond 50% of the indenter penetration within the coating thickness; the substrate interferes with the hardness measurement for soft material deposited on hard material.

Using the previously obtained indentation data in Eq. (2), we were able to evaluate the elastic modulus of the TiO_2/HAP composite. As a result, Fig. 5c is a typical curve representing the elastic modulus variation as a function of the ratio (a/t). In the range of 0–0.25 (a/t) for the indentation penetration lower than 180 nm, we observed some variations in the indentation data related to the insufficient precision of the influence of the indenter tip defect involved in the computation of the contact area. Starting from the limit of $a/t = 0.25$, we noticed an increase in TiO_2/HAP composite elastic modulus (from 7 GPa to 18 GPa) due to medium components precipitation and surface retention, a signature of bioactivity as previously demonstrated. Soaking the TiO_2/HAP composite in medium resulted in an improvement of both hardness up to 0.6 GPa and elastic modulus up to 18 GPa which lies in the domain of human cortical bone [50,51].

4. Conclusion

Using both spin and dip processes we were able to build two different coatings. The TiO_2/HAP bilayer formed by deposition of HAP outer and TiO_2 inner layer, revealed unsatisfactory structural features including bonding failure and surface delamination along with a high surface roughness leading to lack of stem cell adhesion. In contrast, the TiO_2/HAP composite exhibited better structural features and biocompatible properties. Indeed, stem cells attached well onto the surface, proliferated, and presented a polygonal morphology different from the fibroblastic-*like* morphology found on 316L SS. The difference, in cell proliferation rate and morphology, found between TiO_2/HAP composite and 316L SS could be due to a possible proliferation/differentiation switch into bone lineage. Further studies are required to evaluate the early and late (extending culture time) surface related cell behaviour. Moreover, TiO_2/HAP composite improved the corrosion resistance of the 316L SS implant and showed mechanical properties close to that of hard tissue once incubated in physiological conditions for 7 days, highlighting its potential application in hard tissue replacement.

Author disclosure statement

The authors declare no competing financial interests.

Acknowledgements

The authors are very grateful to the staff of Reims Maternity Hospital for providing umbilical cords and the staff of PICT of Reims Champagne Ardenne University for imaging and Raman analysis.

References

[1] M.T. Andani, N.S. Moghaddam, C. Haberland, D. Dean, M.J. Miller, M. Elahinia, Metals for bone implants. Part 1. Powder metallurgy and implant rendering, Acta Biomater. 10 (2014) 4058–4070.
[2] M. Navarro, A. Michiardi, O. Castano, J. Planell, Biomaterials in orthopaedics, J. R. Soc. Interface 5 (2008) 1137–1158.
[3] J.A. Disegi, M.C. Payne, J.E. Field, Stainless steel in bone surgery, Injury 31 (Suppl. 4) (2000) 2–6.
[4] Y. Okazaki, E. Gotoh, T. Manabe, K. Kobayashi, Comparison of metal concentrations in rat tibia tissues with various metallic implants, Biomaterials 25 (2004) 5913–5920.
[5] B. Gervais, A. Vadean, M. Raison, M. Brochu, Failure analysis of a 316L stainless steel femoral orthopedic implant, Case Stud. Eng. Fail. Anal. 5–6 (2016) 30–38.
[6] S.B. Goodman, Z. Yao, M. Keeney, F. Yang, The future of biologic coatings for orthopaedic implants, Biomaterials 34 (2013) 3174–3183.
[7] S. Vahabzadeh, M. Roy, A. Bandyopadhyay, S. Bose, Phase stability and biological property evaluation of plasma sprayed hydroxyapatite coatings for orthopedic and dental applications, Acta Biomater. 17 (2015) 47–55.
[8] E.S. Ghaith, S. Hodgson, M. Sharp, Laser surface alloying of 316L stainless steel coated with a bioactive hydroxyapatite-titanium oxide composite, J. Mater. Sci. Mater. Med. 26 (2015) 83.
[9] D.Y. Kim, M. Kim, H.E. Kim, Y.H. Koh, H.W. Kim, J.H. Jang, Formation of hydroxyapatite within porous TiO(2) layer by micro-arc oxidation coupled with electrophoretic deposition, Acta Biomater. 5 (2009) 2196–2205.
[10] S.V. Dorozhkin, Calcium orthophosphate deposits: preparation, properties and biomedical applications, Mater. Sci. Eng. C 55 (2015) 272–326.
[11] D. Sidane, D. Chicot, S. Yala, S. Ziani, H. Khireddine, A. Iost, X. Decoopman, Study of the mechanical behavior and corrosion resistance of hydroxyapatite sol–gel thin coatings on 316L stainless steel pre-coated with titania film, Thin Solid Films 593 (2015) 71–80.
[12] D. Sidane, H. Khireddine, S. Yala, S. Ziani, F. Bir, D. Chicot, Morphological and mechanical properties of hydroxyapatite bilayer coatings deposited on 316L SS by sol–gel method, Metall. Mater. Trans. B Process Metall. Mater. Process. Sci. 46 (2015) 2340–2347.
[13] C.E. Wen, W. Xu, W.Y. Hu, P.D. Hodgson, Hydroxyapatite/titania sol–gel coatings on titanium–zirconium alloy for biomedical applications, Acta Biomater. 3 (2007) 403–410.
[14] D.M. Liu, Q. Yang, T. Troczynski, Sol-gel hydroxyapatite coatings on stainless steel substrates, Biomaterials 23 (2002) 691–698.
[15] A.H. Choi, B. Ben-Nissan, Sol-gel production of bioactive nanocoatings for medical applications. Part II: current research and development, Nanomedicine 2 (2007) 51–61.
[16] R.I.M. Asri, W.S.W. Harun, M.A. Hassan, S.A.C. Ghani, Z.A. Buyong, Review of hydroxyapatite-based coating techniques: Sol–gel and electrochemical depositions on biocompatible metals, J. Mech. Behav. Biomed. Mater. 57 (2016) 95–108.
[17] P.A. Ramires, A. Romito, F. Cosentino, E. Milella, The influence of titania/hydroxyapatite composite coatings on in vitro osteoblasts behaviour, Biomaterials 22 (2001) 1467–1474.
[18] S. Yugeswaran, A. Kobayashi, A.H. Ucisik, B. Subramanian, Characterization of gas tunnel type plasma sprayed hydroxyapatite–nanostructure titania composite coatings, Appl. Surf. Sci. 347 (2015) 48–56.
[19] I.S. Kim, P.N. Kumta, Sol–gel synthesis and characterization of nanostructured hydroxyapatite powder, Mater. Sci. Eng. B 111 (2004) 232–236.
[20] A. Balamurugan, S. Kannan, S. Rajeswari, Evaluation of TiO2 coatings obtained using the sol–gel technique on surgical grade type 316L stainless steel in simulated body fluid, Mater. Lett. 59 (2005) 3138–3143.
[21] R.J. Barnes, M.S. Dhanoa, S.J. Lister, Standard normal variate transformation and detrending of near-infrared diffuse reflectance spectra, Appl. Spectrosc. 43 (1989) 772–777.
[22] R.H. Telling, Theoretical Strength and Cleavage of Diamond, 1999.
[23] A. Perriot, E. Barthel, Elastic contact to a coated half-space: effective elastic modulus and real penetration, J. Mater. Res. 19 (2004) 600–608.
[24] H. Rammal, J. Beroud, M. Gentils, P. Labrude, P. Menu, H. Kerdjoudj, E. Velot, Reversing charges or how to improve Wharton's jelly mesenchymal stem cells culture on polyelectrolyte multilayer films, Biomed. Mater. Eng. 23 (2013) 299–309.
[25] H.W. Kim, H.E. Kim, V. Salih, J.C. Knowles, Hydroxyapatite and titania sol-gel composite coatings on titanium for hard tissue implants; mechanical and in vitro biological performance, J. Biomed. Mater. Res. B Appl. Biomater. 72 (2005) 1–8.
[26] N. Mohd Daud, N.B. Sing, A.H. Yusop, F.A. Abdul Majid, H. Hermawan, Degradation and in vitro cell–material interaction studies on hydroxyapatite-coated biodegradable porous iron for hard tissue scaffolds, J. Orthop. Transl. 2 (2014) 177–184.
[27] T. Kizuki, M. Ohgaki, M. Katsura, S. Nakamura, K. Hashimoto, Y. Toda, S. Udagawa, K. Yamashita, Effect of bone-like layer growth from culture medium on adherence of osteoblast-like cells, Biomaterials 24 (2003) 941–947.
[28] A.J. Nathanael, Y.M. Im, T.H. Oh, R. Yuvakkumar, D. Mangalaraj, Biomimetic hierarchical growth and self-assembly of hydroxyapatite/titania nanocomposite coatings and their biomedical applications, Appl. Surf. Sci. 332 (2015) 368–378.
[29] W. Pon-On, N. Charoenphandhu, I.M. Tang, J. Teerapornpuntakit, J. Thongbunchoo, N. Krishnamra, Biocomposite of hydroxyapatite-titania rods (HApTiR): physical properties and in vitro study, Mater. Sci. Eng. C Mater. Biol. Appl. 33 (2013) 251–258.
[30] J.Y. Han, Z.T. Yu, L. Zhou, Hydroxyapatite/titania composite bioactivity coating processed by sol–gel method, Appl. Surf. Sci. 255 (2008) 455–458.
[31] M. Malakauskaite-Petruleviciene, Z. Stankeviciute, A. Beganskiene, A. Kareiva, Sol–gel synthesis of calcium hydroxyapatite thin films on quartz substrate using dip-coating and spin-coating techniques, J. Sol-Gel Sci. Technol. 71 (2014) 437–446.
[32] S. Sasikumar, L. Ravy, Influence of needle-like morphology on the bioactivity of nanocrystalline wollastonite: an in vitro study, Int. J. Nanomedicine 129 (2015)http://dx.doi.org/10.2147/IJN.S79986.
[33] W. Xu, W.Y. Hu, M.H. Li, Q.Q. Ma, P.D. Hodgson, C.E. Wen, Sol-gel derived HA/TiO2 double coatings on Ti scaffolds for orthopaedic applications, Trans. Nonferrous Metals Soc. China 16 (2006) 209–216.
[34] V.V. Nosenko, A.M. Yaremko, V.M. Dzhagan, I.P. Vorona, Y.A. Romanyuk, I.V. Zatovsky, Nature of some features in Raman spectra of hydroxyapatite-containing materials: Raman spectra of hydroxyapatite-containing materials, J. Raman Spectrosc. 47 (2016) 726–730.
[35] X. Chen, S.S. Mao, Titanium dioxide nanomaterials: synthesis, properties, modifications, and applications, Chem. Rev. 107 (2007) 2891–2959.
[36] P. Dhaiveegan, N. Elangovan, T. Nishimura, N. Rajendran, Corrosion behavior of 316L and 304 stainless steels exposed to industrial-marine-urban environment: field study, RSC Adv. 6 (2016) 47314–47324.
[37] L.C. Baxter, V. Frauchiger, M. Textor, I. Ap Gwynn, R.G. Richards, Fibroblast and osteoblast adhesion and morphology on calcium phosphate surfaces, Eur. Cell. Mater. 4 (2002) 1–17.
[38] J. Siegel, M. Polívková, N.S. Kasálková, Z. Kolská, V. Svorčík, Properties of silver nanostructure-coated PTFE and its biocompatibility, Nanoscale Res. Lett. 8 (2013) 388.
[39] D.H. Kim, P.P. Provenzano, C.L. Smith, A. Levchenko, Matrix nanotopography as a regulator of cell function, J. Cell Biol. 197 (2012) 351–360.
[40] M.J. Dalby, N. Gadegaard, R. Tare, A. Andar, M.O. Riehle, P. Herzyk, C.D. Wilkinson, R.O. Oreffo, The control of human mesenchymal cell differentiation using nanoscale symmetry and disorder, Nat. Mater. 6 (2007) 997–1003.
[41] H.W. Kim, Y.H. Koh, L.H. Li, S. Lee, H.E. Kim, Hydroxyapatite coating on titanium substrate with titania buffer layer processed by sol–gel method, Biomaterials 25 (2004) 2533–2538.
[42] P. Strąkowska, R. Beutner, M. Gnyba, A. Zielinski, D. Scharnweber, Electrochemically assisted deposition of hydroxyapatite on Ti6Al4V substrates covered by CVD diamond films - coating characterization and first cell biological results, Mater. Sci. Eng. C Mater. Biol. Appl. 59 (2016) 624–635.
[43] A. Bigi, N. Nicoli-Aldini, B. Bracci, B. Zavan, E. Boanini, F. Sbaiz, S. Panzavolta, G. Zorzato, R. Giardino, A. Facchini, G. Abatangelo, R. Cortivo, In vitro culture of mesenchymal cells onto nanocrystalline hydroxyapatite-coated Ti13Nb13Zr alloy, J. Biomed. Mater. Res. A 82 (2007) 213–221.
[44] M.T. Costa, M.A. Lenza, C.S. Gosch, I. Costa, F. Ribeiro-Dias, In vitro evaluation of corrosion and cytotoxicity of orthodontic brackets, J. Dent. Res. 86 (2007) 441–445.
[45] M.A. Costa, M.H. Fernandes, Proliferation/differentiation of osteoblastic human alveolar bone cell cultures in the presence of stainless steel corrosion products, J. Mater. Sci. Mater. Med. 11 (2000) 141–153.
[46] M. Mozafari, E. Salahinejad, S. Sharifi-Asl, D.D. Macdonald, D. Vashaee, Innovative surface modification of orthopaedic implants with positive effects on wettability and *in vitro anti*-corrosion performance, Surf. Eng. 30 (2014) 688–692.
[47] W.C. Oliver, G.M. Pharr, Measurement of hardness and elastic modulus by instrumented indentation: advances in understanding and refinements to methodology, J. Mater. Res. 19 (2004) 3–20.
[48] J. Malzbender, J.M.J. den Toonder, A.R. Balkenende, G. de With, Measuring mechanical properties of coatings: a methodology applied to nano-particle-filled sol–gel coatings on glass, Mater. Sci. Eng. R. Rep. 36 (2002) 47–103.
[49] Z.H. Xu, D. Rowcliffe, Finite element analysis of substrate effects on indentation behaviour of thin films, Thin Solid Films 447–448 (2004) 399–405.
[50] V.P. Mantripragada, B. Lecka-Czernik, N.A. Ebraheim, A.C. Jayasuriya, An overview of recent advances in designing orthopedic and craniofacial implants, J. Biomed. Mater. Res. A 101 (2013) 3349–3364.
[51] X. Wang, S. Xu, S. Zhou, W. Xu, M. Leary, P. Choong, M. Qian, M. Brandt, Y. Min Xie, Topological design and additive manufacturing of porous metals for bone scaffolds and orthopaedic implants: a review, Biomaterials 83 (2016) 127–141.